



Acetylacetonato chelated ruthenium organometallics incorporating imine–phenol function: Spectroscopic, structural, electrochemical and cytotoxicity studies



Suman Mallick^a, Mrinal Kanti Ghosh^a, Ananda Sarkar^b, Samir Jana^c, Arindam Bhattacharyya^c, Sudip Mohapatra^d, Swarup Chattopadhyay^{a,*}

^a Department of Chemistry, University of Kalyani, Kalyani, Nadia 741235, WB, India

^b Department of Physics, Acharya Prafulla Chandra College, New Barrackpore, Kolkata 700131, India

^c Immunology Laboratory, Department of Zoology, University of Calcutta, 35 Ballygunge Circular Road, Kolkata 700019, India

^d Department of Chemistry, Missouri University of S & T, Rolla, MO 65409, USA

ARTICLE INFO

Article history:

Received 14 October 2014

Received in revised form 8 January 2015

Accepted 18 February 2015

Available online 6 March 2015

Keywords:

Ruthenium

Iminium–phenolato

Redox chemistry

Cytotoxicity

Theoretical study

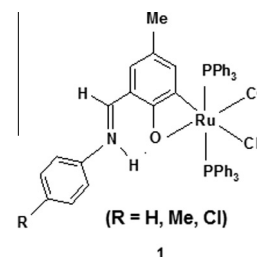
ABSTRACT

The heterogeneous phase reaction of $\text{Ru}(\eta^2\text{-RL})(\text{PPh}_3)_2(\text{CO})\text{Cl}$, **1** with lithium acetylacetonate (Liacac) afforded the complexes of the type $\text{Ru}(\eta^1\text{-RL})(\text{PPh}_3)_2(\text{CO})(\text{acac})$, **2** in excellent yield where $\eta^2\text{-RL}$ is $\text{C}_6\text{H}_2\text{O}-2\text{-CHNHC}_6\text{H}_4\text{R}(p)\text{-3-Me-5}$ and $\eta^1\text{-RL}$ is $\text{C}_6\text{H}_2\text{OH}-2\text{-CHNC}_6\text{H}_4\text{R}(p)\text{-3-Me-5}$ and R is H, Me, Cl. The chelation of acac is attended with the cleavage of Ru–O and Ru–Cl bonds and iminium–phenolato \rightarrow imine–phenol prototropic shift. A sterically controlled change in rotational conformation is involved in the **1** \rightarrow **2** conversion. The conversion is irreversible and the type **2** species are thermodynamically more stable than the carboxylate, nitrite and nitrate complexes of **1**. The crystal structures of $\text{Ru}(\eta^1\text{-MeL})(\text{PPh}_3)_2(\text{CO})(\text{acac})$, **2(Me)** and $\text{Ru}(\eta^1\text{-ClL})(\text{PPh}_3)_2(\text{CO})(\text{acac})$, **2(Cl)** are reported. Spectral (UV–Vis, IR, ^1H NMR) and electrochemical data of the complexes are also reported. The electronic structure and the absorption spectra of the complexes are scrutinized by the density functional theory (DFT) and time-dependent density functional theory (TD-DFT) analyses. The complexes were also screened in vitro for their antiproliferative properties against the MCF-7 breast cancer cell lines by using the MTT assay. Flow cytometric analysis showed that the complexes arrested the cell cycle in the sub G0 phase.

© 2015 Elsevier B.V. All rights reserved.

1. Introduction

The reaction of the Schiff mono bases of 4-methyl-2,6-diformylphenol with $\text{Ru}(\text{PPh}_3)_3\text{Cl}_2$ in ethanol afforded the novel ruthenium organometallics of type $\text{Ru}(\eta^2\text{-RL})(\text{PPh}_3)_2(\text{CO})\text{Cl}$ **1** by decarbonylative orthometallation [1]. The four membered metallacycle incorporating the phenolato function is unprecedented and the CO ligand lies *cis* to the orthometallated carbon where the aldehyde function was attached before decarbonylative metallation. Also notable is the iminium–phenolato zwitterionic function in the six-membered hydrogen bonded chelate ring.



* Corresponding author. Tel.: +91 33 25828750; fax: +91 33 25828282.

E-mail address: icskc@klyuniv.ac.in (S. Chattopadhyay).

The reactivity of these compounds has also been investigated. Complex **1** undergoes facile regiospecific insertion of alkynes into the Ru–C(aryl) bond [2,3] of the four membered metallacycle ring making it six-membered. Isonitriles have also been found to insert into the Ru–O bond of **1** promoting metallacycle expansion [4]. It has also been observed that mono-anionic σ -donor ligands such as carboxylate [5], nitrate, nitrite [6], xanthate [7] and pyridine-2-

thiolate [8] undergo four-membered chelation via displacement of Ru–O and Ru–Cl bonds affording new organometallics. A facile reaction has also been observed between **1** and 2,2'-bipyridine or 1,10-phenanthroline [9] leading to five-membered α -diimine chelation. All the ligands cited above either make four or five-membered chelation with **1**, but none has yet been reported in which six-membered chelation with **1** is present.

In the present work we are exploring the feasibility of introducing a six-membered chelate ring into the organometallic frame of **1** via displacement of Ru–O and Ru–Cl bonds using β -diketonate as the incoming ligand. This ligand choice was based on the reported affinity of β -diketonate for ruthenium [10–14]. A facile reaction has indeed been observed between **1** and lithium acetylacetonate in dichloromethane–acetone–water medium leading to six-membered O,O-chelated organometallics of type $\text{Ru}(\eta^1\text{-RL})(\text{PPh}_3)_2(\text{CO})(\eta^2\text{-acac})$ **2**, the structure and properties of which are described in this work.

Investigations into the development of new anticancer drugs have highlighted ruthenium as a potential metal center [15–17] because ruthenium possesses several favorable properties such as cytotoxicity against cancer cells, similar exchange properties to those of Pt(II) complexes and is easily absorbed and rapidly excreted by the body. It also has reduced toxicity against healthy tissues due to transferrin transport [18,19]. Several ruthenium complexes have displayed promising anticancer activity [20,21]. Cytotoxicity of the complexes of type **1** or its derivatives has not been reported earlier. This has prompted us to examine the cytotoxicity of the complexes of type **2** with the human breast cancer cell line MCF-7 which was evaluated by MTT (3-(4,5-dimethylthiazol-2-yl)-2,5-diphenyltetrazolium bromide) assay. The cell cycle arrest was also analyzed by flow cytometry. We have also examined the effect of different *para*-substituent of the Schiff base ligand ($\eta^1\text{-RL}$) on the antiproliferative effect of the complexes of type **2**.

To get better insight into the electronic structure and optical properties of these complexes, density functional theory (DFT) and time-dependent density functional theory (TD-DFT) studies have also been presented. These combined experimental and theoretical studies provide the first detailed investigation of the electronic structure of the complexes of type **2**.

2. Experimental

2.1. Materials and methods

The compound $\text{Ru}(\eta^2\text{-RL})(\text{PPh}_3)_2(\text{CO})\text{Cl}$ **1** was prepared by the literature method [1]. Lithium acetylacetonate (LiAcac) was purchased from Sigma Aldrich, India. All other reagents were obtained from commercial sources and were used as received. Infrared spectra were recorded on a Perkin-Elmer L120-00A FT-IR spectrometer as a KBr pellet. Electronic spectra were recorded on a Shimadzu UV-1800 PC Spectrophotometer. ^1H NMR spectra were collected on a Bruker DPX-400 spectrometer in CDCl_3 . Microanalyses were performed using a Perkin-Elmer 2400 series-II elemental analyser. Fluorescence spectra were measured on a Perkin-Elmer LS50B spectrofluorimeter. All electrochemical measurements were performed under a nitrogen atmosphere using CHI 600D electrochemistry system. The supporting electrolyte was tetrabutylammonium perchlorate and potentials are referenced to Ag/AgCl electrode.

2.2. Preparation of complexes

The acetylacetonato complexes $\text{Ru}(\eta^1\text{-RL})(\text{PPh}_3)_2(\text{CO})(\eta^2\text{-acac})$ were synthesized by reacting $\text{Ru}(\eta^2\text{-RL})(\text{PPh}_3)_2(\text{CO})\text{Cl}$ **1** with lithium salt of acetylacetonate (LiAcac) in dichloromethane–acetone–water medium. Details of a representative case are given below. The other compounds were prepared analogously.

2.2.1. $\text{Ru}(\eta^1\text{-MeC}_6\text{H}_4\text{L})(\text{PPh}_3)_2(\text{CO})(\eta^2\text{-acac})$, **2(Me)**

To a vigorously stirred solution of $\text{Ru}(\eta^2\text{-MeC}_6\text{H}_4\text{L})(\text{PPh}_3)_2(\text{CO})\text{Cl}$ (100 mg, 0.1094 mmol) in dichloromethane (20 ml) and acetone (20 ml) was added dropwise an aqueous solution of LiAcac (58 mg, 0.5474 mmol). The mixture was then stirred for 3 h when the original violet color of the solution became clear yellow. The organic solvents were then removed under reduced pressure leaving an aqueous suspension of a yellow residue, which was isolated by filtration followed by washing repeatedly with water, and dried in vacuo; yield 97 mg (91%). *Anal. Calc.* for $\text{C}_{57}\text{H}_{51}\text{NO}_4\text{P}_2\text{Ru}$: C, 70.07; H, 5.26; N, 1.43. Found: C, 70.16; H, 5.19; N, 1.45%.

2.2.2. $\text{Ru}(\eta^1\text{-ClC}_6\text{H}_4\text{L})(\text{PPh}_3)_2(\text{CO})(\eta^2\text{-acac})$, **2(Cl)**

This complex was prepared following the same procedure as above using $\text{Ru}(\eta^2\text{-ClC}_6\text{H}_4\text{L})(\text{PPh}_3)_2(\text{CO})\text{Cl}$ as the starting material; yield 95 mg (89%). *Anal. Calc.* for $\text{C}_{56}\text{H}_{48}\text{NO}_4\text{P}_2\text{ClRu}$: C, 67.43; H, 4.85; N, 1.40. Found: C, 67.56; H, 4.93; N, 1.44%.

2.2.3. $\text{Ru}(\eta^1\text{-C}_6\text{H}_5\text{L})(\text{PPh}_3)_2(\text{CO})(\eta^2\text{-acac})$, **2(H)**

$\text{Ru}(\eta^2\text{-C}_6\text{H}_5\text{L})(\text{PPh}_3)_2(\text{CO})\text{Cl}$ was employed as the starting material; yield 96 mg (90%). *Anal. Calc.* for $\text{C}_{56}\text{H}_{49}\text{NO}_4\text{P}_2\text{Ru}$: C, 69.84; H, 5.13; N, 1.45. Found: C, 69.75; H, 5.26; N, 1.52%.

2.3. X-ray crystallography

Single crystals of compositions $\text{Ru}(\eta^1\text{-MeC}_6\text{H}_4\text{L})(\text{PPh}_3)_2(\text{CO})(\eta^2\text{-acac})$ **2(Me)** and $\text{Ru}(\eta^1\text{-ClC}_6\text{H}_4\text{L})(\text{PPh}_3)_2(\text{CO})(\eta^2\text{-acac})$ **2(Cl)** were grown by slow diffusion of hexane into benzene solution of the complexes. The crystals were mounted on a Bruker AXS SMART APEX CCD diffractometer ($\text{Mo K}\alpha$, $\lambda = 0.71073 \text{ \AA}$). The data were reduced in SAINTPLUS [22] and empirical absorption corrections were applied using the SADABS [22] package. The metal atoms were located by the Patterson method and the rest of the non-hydrogen atoms emerged from successive Fourier synthesis. Hydrogen atoms were placed in idealized positions. The structures were refined by a full matrix least-squares procedure on F^2 . All non-hydrogen atoms were refined anisotropically. All calculations were performed using the SHELXTL V6.14 program package [23]. Molecular structure plots were drawn using the Oak Ridge thermal ellipsoid plot ORTEP-32 [24]. The key crystallographic data for **2(Me)** and **2(Cl)** are given in Table 1.

Table 1
Summary of X-ray crystallography for **2(Me)** and **2(Cl)**.

	2(Me)	2(Cl)
Empirical formula	$\text{C}_{57}\text{H}_{51}\text{NO}_4\text{P}_2\text{Ru}$	$\text{C}_{56}\text{H}_{48}\text{ClNO}_4\text{P}_2\text{Ru}$
Formula weight	977.00	997.47
Crystal system	orthorhombic	orthorhombic
Space group	<i>Pbca</i>	<i>Pbca</i>
<i>a</i> (Å)	18.2354(5)	18.094(5)
<i>b</i> (Å)	17.5247(5)	17.500(5)
<i>c</i> (Å)	29.8717(8)	29.358(9)
α (°)	90	90
β (°)	90	90
γ (°)	90	90
<i>V</i> (Å ³)	9546.1(5)	9296(5)
<i>Z</i>	8	8
μ (Mo $\text{K}\alpha$) (mm ⁻¹)	0.444	0.513
Total reflections	153 808	92 381
Independent reflections (R_{int})	10946 (0.0777)	8824 (0.0366)
R_1, wR_2 [$I > 2\sigma(I)$]	0.0391, 0.0841	0.0289, 0.0751
Goodness-of-fit (GOF) on F^2	1.033	1.063
Largest difference in peak and hole (e Å ⁻³)	0.494 and -0.346	0.587 and -0.449

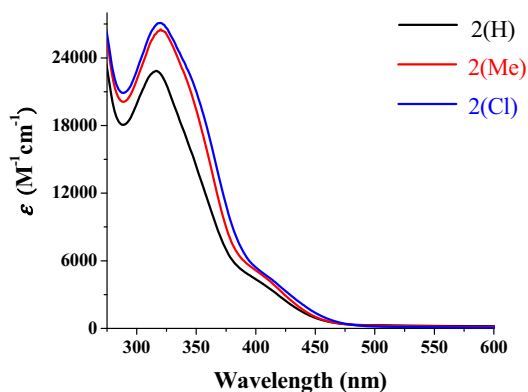


Fig. 1. Absorption spectra of **2**(R) [R = H, Me, Cl] in dichloromethane solution.

2.4. Computer generation of motif 6

The relative positions of CO and the acac chelate were retained as in the structure of **2**(Me) or **2**(Cl) but the phenolic oxygen (O1) (the phenolic C–O length was set at 1.361 Å for **2**(Cl) and 1.358 Å for **2**(Me)) was shifted so as to correspond to the relative position in **1** (R = Me or Cl). The O1...O2 distances are then found to be 2.161 Å in **2**(Cl) and 2.174 Å in **2**(Me).

2.5. Computational study

The molecular geometries of the singlet ground state (S_0) of the synthesized complexes **2**(H) and **2**(Me) have been calculated by the DFT method [25] using the (R)B3LYP hybrid functional approach [26] incorporated into the GAUSSIAN 03 program package [27]. The geometry of the complexes were fully optimized in the gas phase without imposing any symmetry constraints. The single crystal X-ray coordinates of **2**(Me) have been used as the initial input in the calculation. The calculated S_0 structure corresponds nicely to the geometrical parameters obtained experimentally by X-ray diffractometry. On the basis of the optimized ground state geometry, the absorption spectral properties were calculated by the time-dependent density functional theory (TD-DFT) approach [28,29]. The ruthenium atom was described by a double- ζ basis set with the effective core potential of Hay and Wadt (LANL2DZ), and the 6-31+G(d) basis set was used for the other elements present in the complexes to optimize the ground state geometry. The vibrational frequency calculations were performed to ensure that the optimized geometry represents the local minima and that there are only positive eigenvalues. The calculated electronic density plots for frontier molecular orbitals were prepared by using the GaussView 5.0 software. GAUSSSUM 2.1 program was used to calculate the molecular orbital contributions of groups or atoms.

2.6. Cell culture

Human breast cancer MCF-7 cells were obtained from the National Centre for Cell Science, Pune, India and cultured in DMEM supplemented with 10% FCS and antibiotics/antimycotic and gentamycin (50 $\mu\text{g/ml}$) solution with Na-pyruvate (1 mM) in a humidified incubator at 37 °C in 5% CO_2 .

2.7. Phase contrast micrography

Cells were seeded in 24 well culture plates at a density of 1×10^5 cells/well and incubated in DMEM medium containing 10% FCS for 24 h. After attachment of the cells to the plates, the cells were incubated with the complexes **2**(H), **2**(Me) and **2**(Cl) (60–80 μM) for 48 h. After treatment, phase contrast micrographs were taken using a phase contrast microscope (Victory-FL, Dewinter, Italy).

2.8. Cell proliferation-MTT assay

Standard 3-(4,5-dimethylthiazol-2-yl)-2,5-diphenyltetraazolum bromide (MTT) assay procedure was used. Cells were placed in 96-well microassay culture plates (1×10^4 cells per well) in 100 μl DMEM medium and grown overnight for attachment at 37 °C in a 5% CO_2 incubator. After attachment of the cells to the plates, compounds tested [**2**(H), **2**(Me), **2**(Cl)] were then added to the wells to achieve final concentrations ranging from 0 to 120 μM . Control wells were prepared by addition of culture medium (100 μl). The plates were incubated at 37 °C in a 5% CO_2 incubator for 48 h. Upon completion of the incubation, stock MTT dye solution (10 μl , 5 mg/ml) was added to each well and the cells were incubated for a further 4 h. The optical density of each well was then measured with a microplate spectrophotometer at a wavelength of 570 nm. The IC_{50} values were determined by plotting the optical density versus concentration and reading off the concentration at which 50% of cells remain viable relative to the control.

2.9. Cell cycle distribution-flow cytometry

MCF-7 cells were seeded in six-well culture plates at a density of 5×10^5 cells/well and incubated in DMEM medium containing 10% FCS for 24 h. After attachment, the cells were further incubated with the complexes [**2**(H), **2**(Me) and **2**(Cl); 80 μM] for 48 h. After incubation the cell layer was trypsinized and collected by centrifugation at 1500 rpm for 10 min. The cell pellet was fixed with 70% ethanol and then permeabilized with PBS (phosphate buffered saline) solution containing 0.1% triton X-100 with RNase (40 $\mu\text{g/ml}$) for 45 min. The cells were then stained with propidium iodide (PI) solution (50 $\mu\text{g/ml}$) on ice for 30 min. The PI fluorescence was measured through a FL-2 filter (585 nm) using a FACS Verse (BD Biosciences) flow cytometer. Flow cytometry data were analyzed using Cell Quest software.

Table 2

¹H NMR data in CDCl_3 ^{a,b} and UV–Vis spectral data in CH_2Cl_2 .

Compd	δ , ppm								UV–Vis data
	2-H ^s	4-H ^s	O–H ^s	3-Me ^s	16-Me ^s	18-Me ^s	17-H ^s	7-H ^s	λ_{max} , nm (ϵ , $\text{M}^{-1} \text{cm}^{-1}$)
2 (H)	6.19	6.66	12.50	1.72	1.31	1.10	4.40	7.90	409(3761), 317(23055)
2 (Me)	6.26	6.72	12.65	1.79	1.37	1.17	4.47	7.96	413(4047), 322(26137)
2 (Cl)	6.27	6.78	12.39	1.79	1.37	1.18	4.47	7.94	421(3674), 320(27082)

^a Atom numbering is as in Figs. 5 and 6.

^b Aryl protons, 7.00–7.38^m; s = singlet; m = multiplet.

^c Extinction coefficient.

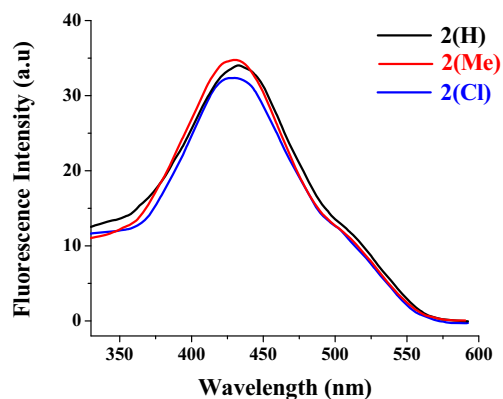


Fig. 2. Emission spectra of 2(R) [R = H, Me, Cl] in dichloromethane solution.

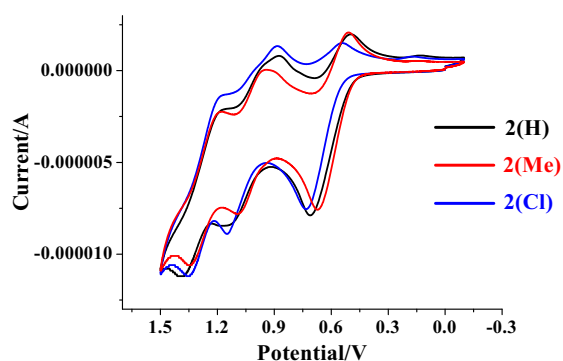
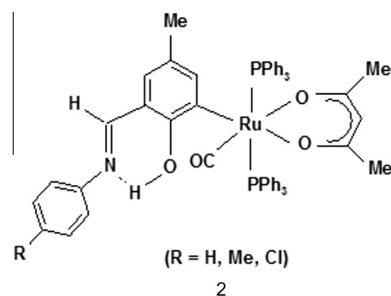


Fig. 3. Cyclic voltammogram of 2(R) [R = H, Me, Cl] in dichloromethane solution recorded at a scan rate of 100 mV s⁻¹.

3. Results and discussion

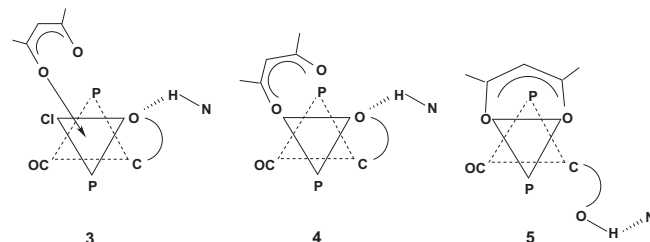
3.1. Synthesis and characterization

In dichloromethane–acetone solution Ru(η^2 -RL)(PPh₃)₂(CO)Cl **1** reacts smoothly with fivefold excess of aqueous lithium acetylacetonate (Liacac) furnishing a yellow solution from which Ru(η^1 -RL)(PPh₃)₂(CO)(η^2 -acac) **2** was isolated as yellow crystalline solid in excellent yield. The η^1 -RL ligand in **2** is a tautomeric form of η^2 -RL ligand [**1**] in **1**. Three different R groups have been used in this work: H, Me and Cl. Specific compounds will be identified by putting R in parenthesis e.g. **2**(H) stands for Ru(η^1 -HL)(PPh₃)₂(CO)(η^2 -acac). The organometallics of type **2** are diamagnetic in agreement with metal oxidation state +2 (idealized t_{2g}⁶). They behave as non electrolytes in acetone, methanol and other common solvents.



The mechanism of the synthetic reaction has not been investigated but a pathway is depicted below on the basis of analogy [5]. It is an

associative pathway in which the acetylacetonate *cis* attack occurs on the chloride atom as in **3**. Once anchored the acac displaces the phenolic oxygen completing the six-membered RuOO chelation (**4,5**). The displaced phenolato ion pulls the originally zwitterionic proton close to it and to avoid steric crowding the monodentate RL ligand rotates around the Ru–C bond (*vide infra*).



In dichloromethane solution the complexes uniformly display two allowed absorption bands in the region 409–421 nm and 317–322 nm, the later being more intense. Electronic spectra of the complexes are shown in Fig. 1 and spectral data are given in Table 2. The solutions of **2** show emission activity, the peak being in the region 429–431 nm, Fig. 2. In IR spectra, the CO stretch appears as a sharp band in the region 1924–1928 cm⁻¹. The C=N stretching frequency in **2** (~1580 cm⁻¹) is significantly lower than that in **1** (~1630 cm⁻¹) [1] as expected which is consistent with the prototropic shift within the salicyaldimine function.

In the ¹H NMR spectra of **2** the 2-H and 4-H resonances of the metallated ring occur as sharp singlets between 6 and 7 ppm. The PPh₃ and Schiff base aromatic protons form a complex multiplet in the region 7.0–7.5 ppm and the azomethine proton occurs as a singlet near 7.9 ppm. The phenolic proton appears as a sharp signal near 12.5 ppm and the signal “disappears” upon shaking with D₂O. This behavior is similar to that of the carboxylate species [5]. Selected ¹H NMR chemical shift data are listed in Table 2.

The present complexes are unreactive towards displacement of acetylacetonate by halide. No reaction was observed upon treatment of **2** with tetraethyl ammonium chloride in acetone-ethanol mixture. This is in contrast to the acetate [5], nitrite and nitrate [6] complexes which are converted to **1** upon treatment with halide. This observation clearly indicates that the six-membered Ru(O,O) ring in **2** is more stable than four-membered Ru(O,O) ring in the acetate, nitrate or nitrite complexes.

3.2. Electrochemical study

All the organometallics of type **2** are electroactive in dichloromethane solution and display three successive cyclic voltammetric responses. Typical voltammograms are shown in Fig. 3 and the potentials versus Ag/AgCl are listed in Table 3. The first oxidation

Table 3
Cyclic voltammetric redox potentials^a and IR spectral data.^b

Compd	Ox1 V (ΔE_p , mV)	Ox2 V (ΔE_p , mV)	Ox3 V (ΔE_p , mV)	IR data:	
				ν_{\max} , cm ⁻¹	C=N C=O
2 (H)	0.61 (210)	1.01 (240)	1.29 (200)	1583 1924	
2 (Me)	0.59 (160)	1.01 (160)	1.27 (150)	1585 1928	
2 (Cl)	0.64 (190)	1.01 (260)	1.26 (170)	1581 1924	

^a Conditions: solvent, dichloromethane; supporting electrolyte, TBAP (0.1 M); working electrode, platinum; reference electrode, Ag/AgCl; solute concentration, $\sim 10^{-3}$ M; $E_{1/2} = 0.5(E_{pa} + E_{pc})$ at scan rate 100 mV s⁻¹, where E_{pa} and E_{pc} are the anodic and cathodic peak potentials, respectively; $\Delta E_p = E_{pa} - E_{pc}$.

^b In KBr disk.

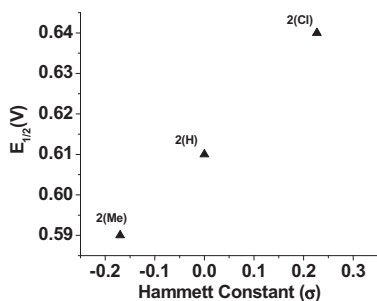


Fig. 4. Plot of Ox1 vs σ_R for the electrochemical transformation of $2(R) \rightarrow 2(R)^+$.

potential (Ox1) values shift marginally to the higher potential as the R-substituent becomes more electron withdrawing. As R is varied, the Ox1 values increase in the Hammett order $\text{Me} < \text{H} < \text{Cl}$. Indeed, the plot of Ox1 versus Hammett constants [30,31] of R are found to be linear [Fig. 4]. According to DFT results the compositions of HOMO and HOMO–1 are metal–ligand mixed centered which indicates that the oxidations are mixed metal–ligand centered. The second (Ox2) and third (Ox3) oxidation potential values do not vary linearly with the Hammett order of the substituents (H, Me, Cl). The acetate [5], nitrate, nitrito [6] and thioxanthato [7] complexes of **1** display only one quasi-reversible cyclic voltammetric response. The presence of three successive cyclic voltammetric responses in the electrochemical experiment of **2** seems to be favored by the strong σ -donor property of the electron rich acetylacetonato ligand.

3.3. Crystal structure

The crystal structures of $\text{Ru}(\eta^1\text{-MeL})(\text{PPh}_3)_2(\text{CO})(\text{acac})$ **2(Me)** and $\text{Ru}(\eta^1\text{-ClL})(\text{PPh}_3)_2(\text{CO})(\text{acac})$ **2(Cl)** have been determined authenticating the binding mode shown in **2**. Molecular views are shown in Figs. 5 and 6 and selected bond parameters are listed in Table 4. The $\text{RuC}_2\text{P}_2\text{O}_2$ coordination sphere has distorted octahedral geometry as can be seen from the angles at the metal center. The Ru, C1, O2, O3 and C40 atoms define an equatorial plane with mean deviation of 0.0647 Å in **2(Me)** and 0.0742 Å in **2(Cl)**. The metallated aldimine ring (Ru, C1 to C7, C14, N1, O1) constitutes a good plane (plane A) with mean deviation of 0.0238 Å in **2(Me)** and 0.0366 Å in **2(Cl)**. The pendant tolyl plane (C8 to C13, C15) in **2(Me)** makes a dihedral angle of 10.2° with plane A whereas for the chlorophenyl ring (C8 to C13, C11) in **2(Cl)** the angle is 7.5° .

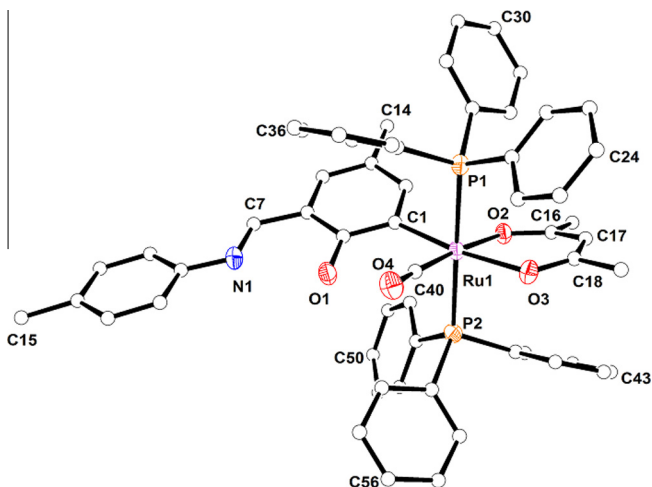
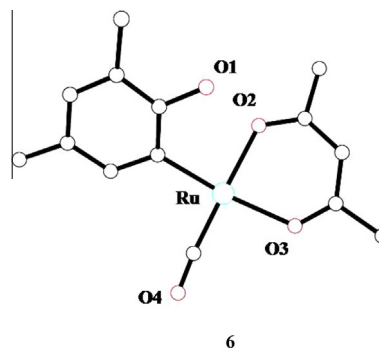


Fig. 5. ORTEP representation of the complex **2(Me)**. Thermal ellipsoids are drawn at the 30% probability level. Hydrogen atoms have been omitted for clarity.

The acetylacetonate chelate ring (Ru, C16 to C20, O2, O3) along with the carbon monoxide ligand and the C1 atom defines a good plane (Plane B) with mean deviation of 0.1233 Å in **2(Me)** and 0.1333 Å in **2(Cl)**. The dihedral angle between plane A and B is 27.6° in **2(Me)** and 29.7° in **2(Cl)**.

The acac ligand is chelated and the Schiff base ligand is monodentate, bonded at the C1 atom only. The PPh_3 ligands lie in *trans* positions (P1–Ru–P2, $178.95(3)^\circ$ in **2(Me)** and $178.263(17)^\circ$ in **2(Cl)**). The phenolic oxygen atom is too far away ($\text{Ru}\cdots\text{O1}$, 3.376 Å in **2(Me)** and 3.350 Å in **2(Cl)**) for metal binding. Acetylacetonate chelation has cleaved the Ru–O(phenolato) bond of the precursor complex **1**. As a result the Schiff base fragment tautomerizes from iminium–phenolato in **1** to imine–phenol in **2**. The N \cdots O distances in **2(Me)** and **2(Cl)** are 2.618 Å and 2.608 Å respectively. The relative orientation of the Schiff base ligand in **2** is different from that in **1**. In **2** the carbonyl group is positioned on the same side of the Schiff base ligand as the uncoordinated phenolic function. While in **1** the carbonyl group lies *trans* to the coordinated phenolic function. In effect the Schiff base ligand has undergone a large rotation around the Ru–C(aryl) bond in going from **1** \rightarrow **2**. This rotation and the consequent distancing of the phenolic function from coordinated acetylacetonate is consistent with steric consideration. If the phenolic oxygen was placed at the carbon site close to the acetylacetonate function (O2 in particular) the situation depicted in **6** will arise.



Here the $\text{O1}\cdots\text{O2}$ distance would be 2.161 Å in **2(Cl)** and 2.174 Å in **2(Me)**. The van der Waals radius of oxygen is 1.4 Å [32,33]. Clearly strong $\text{O1}\cdots\text{O2}$ repulsion is present in **6** and this is believed to lead to rotation of the phenolic function to the position in **2** where the

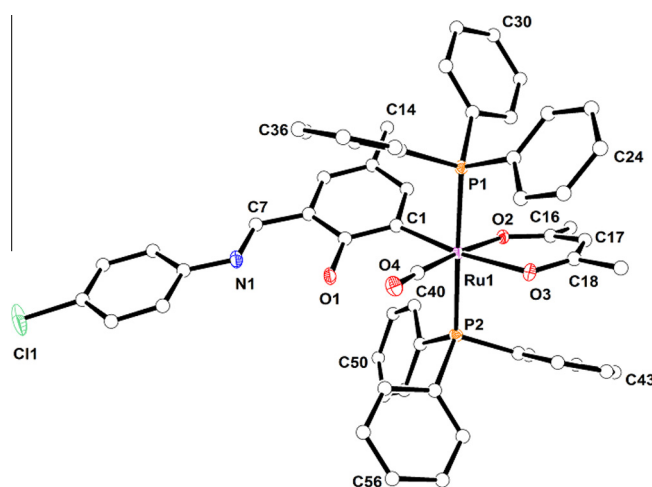


Fig. 6. ORTEP representation of the complex **2(Cl)** with thermal ellipsoids drawn at the 30% probability level. Hydrogen atoms have been omitted for clarity.

Table 4Selected bond distances (Å) and angles (°) and their estimated standard deviations for **2**(Me) and **2**(Cl).

	2 (Me)	2 (Cl)
<i>Distances</i>		
Ru1–P1	2.4138(8)	2.4160(8)
Ru1–P2	2.3992(8)	2.3955(8)
Ru1–O2	2.1287(18)	2.1309(13)
Ru1–O3	2.166(2)	2.1604(14)
Ru1–C40	1.822(3)	1.8248(19)
Ru1–C1	2.089(3)	2.0908(19)
O3–C18	1.268(4)	1.268(2)
O2–C16	1.275(3)	1.279(2)
C17–C18	1.386(4)	1.399(3)
C17–C16	1.385(4)	1.392(3)
C7–N1	1.269(4)	1.283(3)
<i>Angles</i>		
P1–Ru1–P2	178.95(3)	178.263(17)
C1–Ru1–O3	171.97(9)	171.55(6)
C40–Ru1–O2	175.62(11)	175.64(7)
O2–Ru1–O3	85.69(7)	86.39(5)
C1–Ru1–C40	94.35(12)	94.16(8)
C40–Ru1–O3	92.11(11)	92.15(7)
C1–Ru1–O2	88.17(9)	87.72(6)
Ru1–C40–O4	174.6(3)	174.85(16)

Table 5Selected DFT optimized geometrical parameters (bond lengths (Å) and angles (°)) of **2**(H) and **2**(Me) in the ground state.

	2 (H)	2 (Me)
<i>Distances (Å)</i>		
Ru1–P1	2.424	2.467
Ru1–P2	2.452	2.491
Ru1–O2	2.167	2.186
Ru1–O3	2.197	2.229
Ru1–C40	1.838	1.849
Ru1–C1	2.111	2.117
O3–C18	1.279	1.266
O2–C16	1.290	1.278
C17–C18	1.423	1.415
C17–C16	1.412	1.402
C7–N1	1.309	1.297
<i>Angles (°)</i>		
P1–Ru1–P2	177.72	176.91
C1–Ru1–O3	171.99	172.81
C40–Ru1–O2	175.74	173.66
O2–Ru1–O3	85.57	83.94
C1–Ru1–C40	96.59	96.39
C40–Ru1–O3	90.87	90.23
C1–Ru1–O2	87.09	89.55
Ru1–C40–O4	172.53	171.67

O1...O2 and O1...O3 distances are 4.950 Å and 5.272 Å, respectively in **2**(Me) and 4.910 Å and 5.236 Å, respectively in **2**(Cl). The *trans* influence of the metallated carbanionic site C1 is expected to lengthen the Ru–O3 distance compare to Ru–O2 distance. Indeed, the Ru–O3 distance is slightly longer than the Ru–O2 distance in both **2**(Me) and **2**(Cl). In chelated acetylacetonates the Ru^{II}–O bond lengths usually lie in the range 1.99–2.08 Å [10–14]. The Ru^{II}–O bond lengths in **2**(Me) and **2**(Cl) [Ru–O2: 2.129 Å in **2**(Me) and 2.131 Å in **2**(Cl); Ru–O3: 2.166 Å in **2**(Me) and 2.160 Å in **2**(Cl)] are slightly longer than that observed in other structurally characterized Ru^{II}–acetylacetonate species [10–14]. The similarities in the two C–O and two C–C distances in the acetylacetonate frame in both **2**(Me) and **2**(Cl) correspond to a delocalized situation.

3.4. DFT study and computational details

In spite of several attempts, we were unable to grow the X-ray quality single crystals of the complex **2**(H). The geometrical structures of the singlet ground state (t_{2g}^6) of **2**(H) along with **2**(Me) were optimized by the DFT [25] method with B3LYP exchange correlation functional [26] approach. The geometry used for the ground state optimization is based on the crystal structure parameters of complex **2**(Me) without any ligand simplification and symmetry constraints. Since the three complexes have very similar spectroscopic and cyclic voltammetric properties (*vide supra*) which implies a close similarity between their electronic and molecular structures, the absorption spectral property of one

representative complex, **2**(Me) was calculated by time dependent density functional theory (TD-DFT) [28,29] approach on the basis of the optimized ground state geometry. For many transition metal complexes, the TD-DFT approach had been found to be reliable for calculating spectral properties [34,35]. TD-DFT method provides more accurate electronic excitation energies because of the presence of electronic correlation.

The geometry optimized structures of **2**(H) and **2**(Me) have been depicted in Fig. 7 and the significant metrical parameters are listed in Table 5. The optimized geometries of the complexes do not show significant differences in the coordination sphere around the ruthenium center which means that the ligands bind in a similar fashion in the complexes. The optimized structural parameters of the complexes are in general agreement with the experimental values (Table 4) and the slight discrepancy (maximum deviation 0.0918 Å for Ru–P2 bond distance) arises due to the crystal lattice distortion existing in the real molecule. The isodensity plots from HOMO–5 to LUMO+5 are shown in Fig. 8 and partial frontier molecular orbital compositions and energy levels are listed in Table 6. The compositions of HOMOs and LUMOs are important in understanding the nature of transition in the absorption spectra of the complexes. HOMO is mainly composed of RL ligand π -orbital (60.4%) and filled *d*-orbital of Ru (29.75%) while LUMO is mainly composed of RL ligand π^* orbital (78.95%). The relative energy levels of FMOs are depicted in Fig. 9.

The calculated charge on the ruthenium atom is considerably lower than the formal charge of +2 (Table 7). This is due to the significant charge donation from the C_{aryl}, C_{carbonyl}, P_{phosphine} and

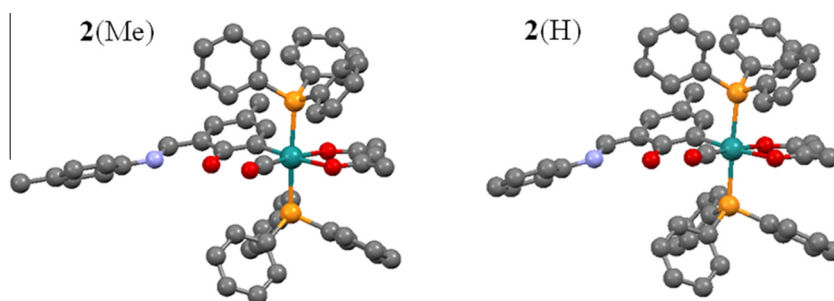


Fig. 7. Optimized molecular structures of **2**(Me) and **2**(H). [C: Grey, N: Sky Blue, O: Red, P: Orange, Ru: Green]. All hydrogen atoms are omitted for clarity. (For interpretation of the references to colour in this figure legend, the reader is referred to the web version of this article.)

O_{acetylacetonato} donors. The charge on the C_{aryl} atom is significantly lower than –1 indicating that there is higher electron density delocalization from the C_{aryl} to ruthenium center.

The computed vertical transitions were calculated at the equilibrium geometry of the S₀ state and described in term of one-electron excitations of the molecular orbitals of the corresponding S₀ geometry. The calculated absorption energies associated with their oscillator strengths, the main configurations and their assignments as well as the experimental data for **2**(Me) are given in Table 8.

For **2**(Me) mainly two transitions have been observed going from the lower to the higher energy region of the spectra. The low energy transition is observed near 413 nm as broad band. This feature is analyzed and it is in excellent agreement with the absorptions at 402.58 nm (3.079 eV, $f = 0.0605$) which is due to the H → L (89%) transition and it is assigned to the $[d(\text{Ru}) \pi(\text{RL})] \rightarrow [\pi^*(\text{RL}) + \pi^*(\text{PPh}_3)]$ character and is mainly ILCT in nature.

The other experimentally observed absorption in the UV region at 322 nm comprises the excitations at 345.50 nm (3.589 eV,

$f = 0.2146$) and 340.55 nm (3.641 eV, $f = 0.1628$). The first transition is mainly due to the H–3 → L+1 (12%), H–1 → L (45%) and H–1 → L+1 (17%) transitions and can be ascribed to $[d(\text{Ru}) + p(\text{O}_{\text{acac}}) + \pi(\text{CO})] \rightarrow [d(\text{Ru}) + \pi^*(\text{PPh}_3)]$, $[d(\text{Ru}) + p(\text{O}_{\text{acac}}) + \pi(\text{RL})] \rightarrow [\pi^*(\text{RL}) + \pi^*(\text{PPh}_3)]$ and $[d(\text{Ru}) + p(\text{O}_{\text{acac}}) + \pi(\text{RL})] \rightarrow [d(\text{Ru}) + \pi^*(\text{PPh}_3)]$ transitions. The second one appeared as a linear combination of H–2 → L+1 (19%), H–1 → L (22%) and H–1 → L+1 (30%) transitions and they are assigned primarily to the $[p(\text{O}_{\text{acac}}) + \pi(\text{RL}) + \pi(\text{PPh}_3)] \rightarrow [d(\text{Ru}) + \pi^*(\text{PPh}_3)]$, $[d(\text{Ru}) + p(\text{O}_{\text{acac}}) + \pi(\text{RL})] \rightarrow [\pi^*(\text{RL}) + \pi^*(\text{PPh}_3)]$ and $[d(\text{Ru}) + p(\text{O}_{\text{acac}}) + \pi(\text{RL})] \rightarrow [d(\text{Ru}) + \pi^*(\text{PPh}_3)]$ transitions. Those transitions are essentially MLCT, LLCT and ILCT in nature.

3.5. Cytotoxicity

The cytotoxicity of the complexes **2**(H), **2**(Me) and **2**(Cl) to human breast cancer cell line MCF-7 was assayed by cell survival after 48 h of exposure to the desired concentration range (0–120 μM) using the MTT assay which is depicted in Fig. 10. It

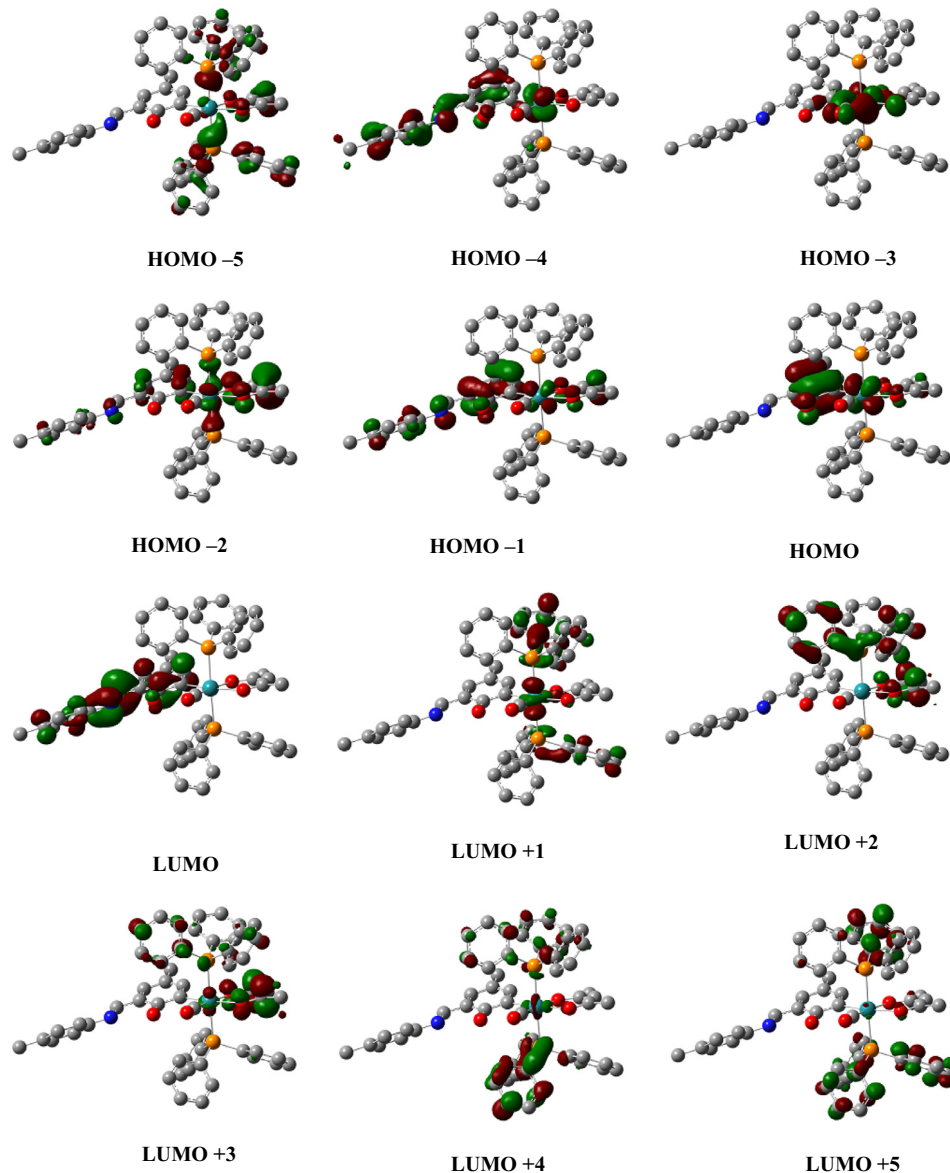


Fig. 8. Isodensity plot of frontier molecular orbitals of **2**(Me) with isodensity value 0.04.

Table 6
Frontier molecular orbital composition (%) in the ground state for **2(Me)**.

Orbital	Energy (eV)	Contribution (%)					Main bond type
		Ru	PPh ₃	O _{acac}	RL	CO	
LUMO+5	-0.416	1.49	92.62	4.40	0.26	1.23	$\pi^*(\text{PPh}_3)$
LUMO+4	-0.472	5.18	91.35	1.15	1.38	0.94	$\pi^*(\text{PPh}_3)$
LUMO+3	-0.554	3.37	44.53	51.42	0.41	0.27	$\pi^*(\text{PPh}_3) + \pi^*(\text{O}_{\text{acac}})$
LUMO+2	-0.610	0.27	62.07	32.62	0.38	4.66	$\pi^*(\text{PPh}_3) + \pi^*(\text{O}_{\text{acac}})$
LUMO+1	-0.887	19.00	71.72	4.73	2.32	2.23	$d(\text{Ru}) + \pi^*(\text{PPh}_3)$
LUMO	-1.156	0.19	20.56	0.25	78.95	0.05	$\pi^*(\text{RL}) + \pi^*(\text{PPh}_3)$
HOMO	-4.770	29.75	2.21	7.32	60.40	0.32	$d(\text{Ru}) + \pi(\text{RL})$
HOMO-1	-5.175	11.02	3.7	15.47	69.69	0.12	$d(\text{Ru}) + p(\text{O}_{\text{acac}}) + \pi(\text{RL})$
HOMO-2	-5.411	8.05	15.58	45.16	30.15	1.06	$p(\text{O}_{\text{acac}}) + \pi(\text{RL}) + \pi(\text{PPh}_3)$
HOMO-3	-5.638	67.44	1.02	14.29	3.75	13.5	$d(\text{Ru}) + p(\text{O}_{\text{acac}}) + \pi(\text{CO})$
HOMO-4	-6.030	22.07	5.74	2.82	68.58	0.79	$d(\text{Ru}) + \pi(\text{RL})$
HOMO-5	-6.148	7.55	76.04	15.76	0.27	0.38	$p(\text{O}_{\text{acac}}) + \pi(\text{PPh}_3)$

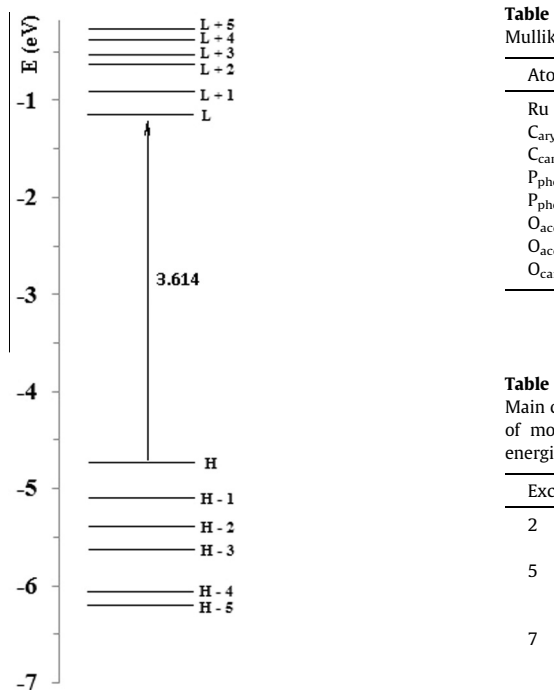


Fig. 9. Partial molecular orbital diagram for complex **2(Me)**. The arrow is intended to highlight the HOMO–LUMO energy gap. The DFT energy value is given in eV.

has been found that increasing complex concentrations decrease the MCF-7 cell viability in a dose-dependent manner. The IC₅₀ values obtained after 48 h of drug treatment with the MTT assay are found to be around 80 μM .

To further observe and study the antitumor activity of these ruthenium complexes, morphological study was performed. Cell death was characterized by obvious morphological characteristics. MCF-7 cells treated with the ruthenium complexes showed clear morphological change and quantity decrease, as shown in Fig. 11. The morphological change of the cells is positively correlated with dosage. These phenomena suggest that the ruthenium complexes block the growth of MCF-7 cells. The detachment of cells from the substratum, change of cell morphology and cell shrinkage were clearly observed which points to the cell death after 48 h exposure of the compounds on MCF-7 cells.

Inhibition of cancer-cell proliferation by cytotoxic drugs could be the result of cell cycle arrest [36,37]. According to the result of the MTT assay, complexes of type **2** are active in inhibiting MCF-7 cell growth. Thus, these complexes were used for further investigation of the underlying mechanism. The effect of the complexes [**2(H)**, **2(Me)**, **2(Cl)**] on the cell cycle of MCF-7 cells were

Table 7
Mulliken atomic charges for **2(Me)**.

Atom	Atomic charges
Ru	-0.134606
C _{aryl}	-0.058835
C _{carbonyl}	0.243174
P _{phosphine}	0.614004
P _{phosphine}	0.635973
O _{acetylacetonato}	-0.518311
O _{acetylacetonato}	-0.481334
O _{carbonyl}	-0.302586

Table 8
Main calculated optical transitions for the complex **2(Me)** with composition in terms of molecular orbital contribution of the transition, computed vertical excitation energies and oscillator strength (*f*).

Excitation	Composition	<i>E</i> (eV)	<i>f</i>	λ_{theo} (nm)	Assign	λ_{exp} (nm)
2	H \rightarrow L (89%)	3.079	0.0605	402.58	ILCT	413
5	H-3 \rightarrow L+1 (12%) H-1 \rightarrow L (45%) H-1 \rightarrow L+1 (17%)	3.589	0.2146	345.50	MLCT ILCT LLCT	322
7	H-2 \rightarrow L+1 (19%) H-1 \rightarrow L (22%) H-1 \rightarrow L+1 (30%)	3.641	0.1628	340.55	LLCT ILCT LLCT	

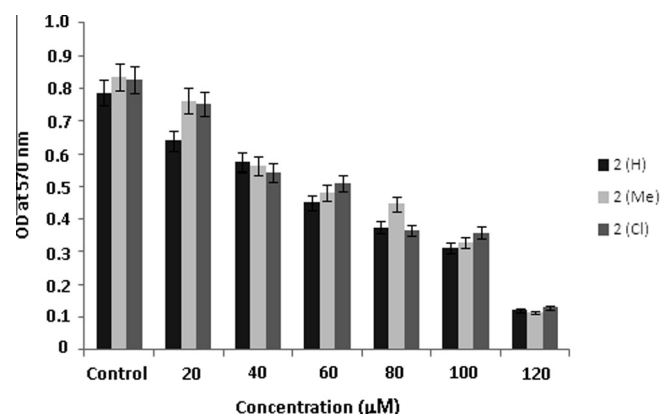


Fig. 10. Growth inhibitory effect of the complex **2(R)** on MCF-7 cells.

studied by flow cytometry in propidium iodide (PI)-stained cells after treatment with the complexes for 48 h to determine the possible mechanism of cell-growth inhibition. The representative DNA

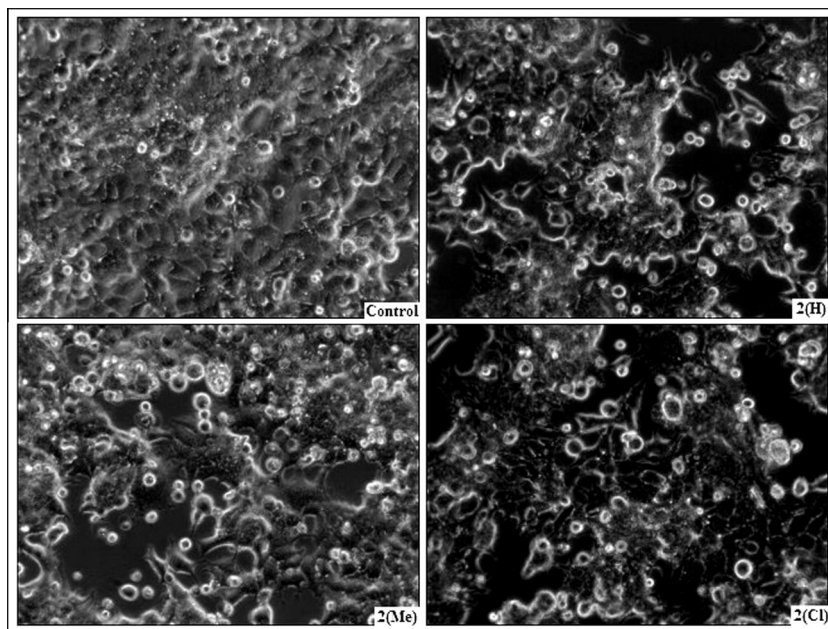


Fig. 11. Phase contrast micrographs (20× magnifications) of MCF-7 cells after exposure of **2**(R) for 48 h.

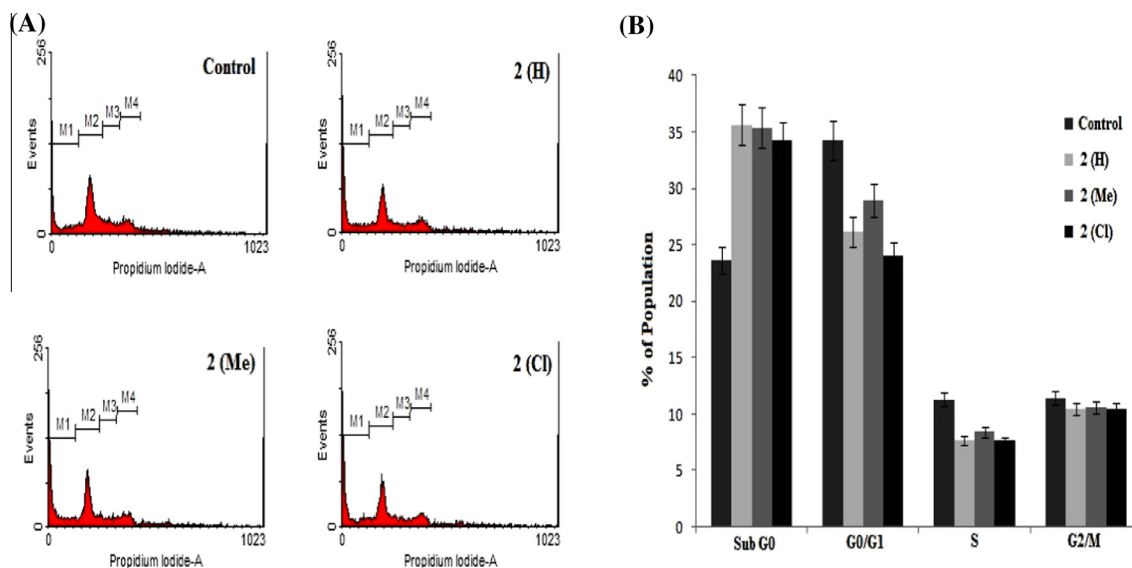


Fig. 12. Flow cytometry analysis of the cell cycle distribution of MCF-7 cells after exposure of **2**(R) for 48 h.

distribution histograms of MCF-7 cells in the absence and presence of the complexes are shown in Fig. 12. The cell cycle distribution pattern shows an obvious enhancement (~12%) in the percentage of cells at sub G0 phase accompanied by reduction in the percentage of cells in the G0/G1 phase and S phase. Increase in the percentage of cells at the sub G0 phase clearly indicates the induction of sub G0 phase arrest by complexes of type **2**.

We were expecting that the cytotoxic properties of the complexes of type **2** should correlate somewhat with the electronic nature [38] of the three different *para*-substituents (H, Me, Cl) on the η^1 -RL ligand but the IC₅₀ values obtained after 48 h of drug treatment are found to be around 80 μ M (Fig. 10) for all the three complexes. Flow cytometry analysis also shows the similar cell cycle distribution pattern for **2**(H), **2**(Me) and **2**(Cl). So the MTT cell proliferation assay and flow cytometry analysis experiments show

that the *para*-substituents on the η^1 -RL ligand do not induce any change in the antiproliferative activity of the complexes of type **2**.

4. Conclusions

The main finding of this work will now be summarized. It is demonstrated that Ru(η^2 -RL)(PPh₃)₂(CO)Cl **1** undergoes facile substitution of chloride by acetylacetonate affording a new family of aryl ruthenium species, Ru(η^1 -RL)(PPh₃)₂(CO)(acac) **2**. The complexes are characterized by different spectroscopic techniques, elemental analysis and X-ray structure determination. Structure determination has revealed that in going from **1** → **2** the RL ligand changes its hapticity from η^2 to η^1 as the iminium–phenolato function tautomerizes to the imine–phenol function. In **2** the metallated

aryl ring is turned away from the acac chelate plane due to the steric repulsion between acac and phenolic oxygen atoms and this leads to the rotameric *anti* → *syn* isomerization of the phenolic C–O function with respect to the coordinated carbon monoxide. In vitro cytotoxicity experiments show that the complexes have growth-inhibitory effect on MCF-7 cells, inducing sub G0 cell-cycle arrest. To gain better insight into the geometry and electronic structures of the complexes density functional theory (DFT) and time-dependent DFT (TD-DFT) calculations were performed. This provides, for the first time, a detailed assignment of the significant spectral features of the investigated complexes. The computed vertical excitation energies are in good agreement with the experimental ones. Our search for new aryl ruthenium(II) complexes with different chelating ligands and their characterization are continuing.

Acknowledgments

Financial support from the Department of Science and Technology, Government of India (No. SR/S1/IC-65/2010) is gratefully acknowledged. University of Kalyani for infrastructural facilities. The support of DST under FIST program to the Department of Chemistry and PURSE to the University of Kalyani is also acknowledged. We are also thankful to Dr. Rajat Saha of Jadavpur University for help with the crystallography. S.M. thanks UGC, India and M. K. G. thanks University of Kalyani for the pre-doctoral fellowships.

Appendix A. Supplementary material

CCDC 991302 and 991303 contains the supplementary crystallographic data for **2**(Me) and **2**(Cl), respectively. These data can be obtained free of charge from The Cambridge Crystallographic Data Centre via www.ccdc.cam.ac.uk/data_request/cif. Supplementary data associated with this article can be found, in the online version, at <http://dx.doi.org/10.1016/j.ica.2015.02.023>.

References

- [1] P. Ghosh, N. Bag, A. Chakravorty, *Organometallics* 15 (1996) 3042.
- [2] K. Ghosh, S. Chattopadhyay, S. Pattanayak, A. Chakravorty, *Organometallics* 20 (2001) 1419.
- [3] S. Chattopadhyay, K. Ghosh, S. Pattanayak, A. Chakravorty, *J. Chem. Soc., Dalton Trans.* (2001) 1259.
- [4] B.K. Panda, S. Chattopadhyay, K. Ghosh, A. Chakravorty, *Organometallics* 21 (2002) 2773.
- [5] P. Ghosh, A. Pramanik, A. Chakravorty, *Organometallics* 15 (1996) 4147.
- [6] P. Ghosh, A. Chakravorty, *Inorg. Chem.* 36 (1997) 64.
- [7] S. Chattopadhyay, B.K. Panda, K. Ghosh, A. Chakravorty, *Israel J. Chem.* 41 (2001) 139.
- [8] B.K. Panda, S. Chattopadhyay, K. Ghosh, A. Chakravorty, *Polyhedron* 21 (2002) 899.
- [9] B.K. Panda, K. Ghosh, S. Chattopadhyay, A. Chakravorty, *J. Organomet. Chem.* 674 (2003) 107.
- [10] S. Chatterjee, S. Mandal, S. Joy, C.-H. Hung, S. Goswami, *Inorg. Chim. Acta* 374 (2011) 366.
- [11] D. Das, B. Sarkar, D. Kumbhakar, T.K. Mondal, S.M. Mobin, J. Fiedler, F.A. Urbanos, R.J. Aparicio, W. Kaim, G.K. Lahiri, *Chem. Eur. J.* 17 (2011) 11030.
- [12] P. Mondal, F. Ehret, M. Bubrin, A. Das, S.M. Mobin, W. Kaim, G.K. Lahiri, *Inorg. Chem.* 52 (2013) 8467.
- [13] S. Kar, N. Chanda, S.M. Mobin, A. Datta, F.A. Urbanos, V.G. Puranik, R.J. Aparicio, G.K. Lahiri, *Inorg. Chem.* 43 (2004) 4911.
- [14] (a) P.N. Liu, Z.Y. Zhou, C.P. Lau, *Chem. Eur. J.* 13 (2007) 8610; (b) M.A. Bennett, G.A. Heath, D.C.R. Hockless, I. Kovacic, A.C. Willis, *J. Am. Chem. Soc.* 120 (1998) 932; (c) M.A. Bennett, G.A. Heath, D.C.R. Hockless, I. Kovacic, A.C. Willis, *Organometallics* 17 (1998) 5867.
- [15] J.M. Rademaker-Lakhai, B.D. Van, D. Pluim, J.H. Beijnen, J.H. Schellens, *Clin. Cancer Res.* 10 (2004) 3717.
- [16] C.G. Hartinger, S. Zorbas-Seifried, M.A. Jakupec, B. Kynast, H. Zorbas, B.K. Keppler, *J. Inorg. Biochem.* 100 (2006) 891.
- [17] C.G. Hartinger, M.A. Jakupec, S. Zorbas-Seifried, M. Groessl, A. Egger, W. Berger, H. Zorbas, P.J. Dyson, B.K. Keppler, *Chem. Biodiversity* 5 (2008) 2140.
- [18] P.C. Bruijninx, P.J. Sadler, *Curr. Opin. Chem. Biol.* 12 (2008) 197.
- [19] M.A. Jakupec, M. Galanski, V.B. Arion, C.G. Hartinger, B.K. Keppler, *J. Chem. Soc., Dalton Trans.* (2008) 183.
- [20] L. Bratsos, S. Jedner, T. Gianferrara, E. Alessio, *Chimia* 61 (2007) 692.
- [21] X.J. Meng, M.L. Leyva, M. Jenny, I. Gross, S. Benosman, B. Fricker, S. Harlepp, P. Hebraud, A. Boos, P. Wlosik, *Cancer Res.* 69 (2009) 5458.
- [22] SMART; SAINT; SADABS; XPREP; SHELXTL, Bruker AXS Inc., Madison, WI, 1998.
- [23] G.M. Sheldrick, SHELXTL, v. 6.14, Bruker AXS Inc., Madison, WI, 2003.
- [24] C.K. Johnson, ORTEP Report ORNL-5138, Oak Ridge National Laboratory, Oak Ridge, TN, 1976.
- [25] E. Runge, E.K.U. Gross, *Phys. Rev. Lett.* 52 (1984) 997.
- [26] A.D. Becke, *J. Chem. Phys.* 98 (1993) 5648.
- [27] M.J. Frisch, G.W. Trucks, H.B. Schlegel, G.E. Scuseria, M.A. Robb, J.R. Cheeseman, J.A. Montgomery Jr., T. Vreven, K.N. Kudin, J.C. Burant, J.M. Millam, S.S. Iyengar, J. Tomasi, V. Barone, B. Mennucci, M. Cossi, G. Scalmani, N. Rega, G.A. Petersson, H. Nakatsuji, M. Hada, M. Ehara, K. Toyota, R. Fukuda, J. Hasegawa, M. Ishida, T. Nakajima, Y. Honda, O. Kitao, H. Nakai, M. Klene, X. Li, J.E. Knox, H.P. Hratchian, J.B. Cross, V. Bakken, C. Adamo, J. Jaramillo, R. Gomperts, R.E. Stratmann, O. Yazyev, A.J. Austin, R. Cammi, C. Pomelli, J.W. Ochterski, P.Y. Ayala, K. Morokuma, G.A. Voth, P. Salvador, J.J. Dannenberg, V.G. Zakrzewski, S. Dapprich, A.D. Daniels, M.C. Strain, O. Farkas, D.K. Malick, A.D. Rabuck, J. Raghavachari, J.B. Foresman, J.V. Ortiz, Q. Cui, A.G. Baboul, S. Clifford, J. Cioslowski, B.B. Stefanov, G. Liu, A. Liashenko, P. Piskorz, I. Komaromi, R.L. Martin, D.J. Fox, T. Keith, M.A. Al-Laham, C.Y. Peng, A. Nanayakkara, M. Challacombe, P.M.W. Gill, B. Johnson, W. Chen, M.W. Wong, C. Gonzalez, J.A. Pople, *GAUSSIAN 03*, Revision D.01, Gaussian Inc., Wallingford, CT, 2004.
- [28] K.L. Bak, P. Jorgensen, T. Helgaker, K. Rund, H.J.A. Jensen, *J. Chem. Phys.* 98 (1993) 8873.
- [29] J. Autschbach, T. Ziegler, S.J.A. Gisbergen, E.J. Baerends, *J. Chem. Phys.* 116 (2002) 6930.
- [30] L.P. Hammett, *Physical Organic Chemistry*, second ed., Mc Graw-Hill, New York, 1970.
- [31] I.L. Finar, *Organic Chemistry*, vol-I: Fundamental Principles, sixth ed., ELBS, Longman Group, Essex, England, 1990. p. 605.
- [32] L. Pauling, *The Nature of the Chemical Bond and the Structure of Molecules and Crystals*, third ed., Cornell University Press, Ithaca, NY, 1960.
- [33] A.K. Rappe, C.J. Casewit, K.S. Colwell, W.A. Goddard, W.M. Skiff, *J. Am. Chem. Soc.* 114 (1992) 10024.
- [34] T. Liu, H.-X. Zhang, B.-H. Xia, *J. Phys. Chem. A* 111 (2007) 8724.
- [35] X. Zhou, A.-M. Ren, J.-K. Feng, *J. Organomet. Chem.* 690 (2005) 338.
- [36] T.F. Chen, Y.N. Liu, W.J. Zheng, J. Liu, Y.S. Wong, *Inorg. Chem.* 49 (2010) 6366.
- [37] T.F. Chen, Y.S. Wong, *J. Agric. Food Chem.* 56 (2008) 10574.
- [38] O. Zekri, E.A. Hillard, S. Top, A. Vessieres, P. Pigeon, M.-A. Plamont, M. Huche, S. Boutamine, M.J. McGlinchey, H. Muller-Bunz, G. Jaouen, *J. Chem. Soc., Dalton Trans.* (2009) 4318.